

Investigation of a New Macroscopic Model of
Traffic Flow

Kate Alexander

Abstract

The study of traffic flow as given rise to many models aiming to realistically predict the behaviour of traffic. Here we discuss a macroscopic method, closely related to the Bando [1] microscopic model. A similarity solution is found for the inhomogeneous case and the homogeneous case is solved for a Riemann problem. We use Roe decomposition with the first order upwind scheme to find a numerical solution and investigate the effect of the source and relaxation terms on the system.

Declaration

I confirm that this is my own work and the use of all materials from other sources has been properly and fully acknowledged.

Signed

Acknowledgements

I would like to thank my supervisors Professor Mike Baines and Dr Peter Sweby for their help with this project. I am very grateful for all their encouragement, endless patience and for Mike's fabulous sense of humour. I am also very grateful to Sue Davis, Jo Morgan and my fellow M.Sc. students for their support.

I would also like to thank the EPSRC for their financial support throughout this course.

Contents

- 1 Introduction** **1**

- 2 Traffic Models** **3**
 - 2.1 Microscopic Models 3
 - 2.1.1 The Bando Model 4
 - 2.2 Macroscopic Models 5
 - 2.2.1 The BMW Model 7

- 3 A New Macroscopic Model** **11**
 - 3.1 A Similarity Solution 12

- 4 The Homogeneous System** **16**
 - 4.1 The Riemann Solution 18
 - 4.1.1 Different Initial Data 23

- 5 The Numerical Method** **25**
 - 5.1 Roe Decomposition 25
 - 5.2 The Roe Scheme 28
 - 5.2.1 Accuracy and Stability 28
 - 5.2.2 Boundary Conditions 29
 - 5.3 The Data 29

- 6 Numerical Results** **30**
 - 6.1 The Homogeneous System 30
 - 6.2 The Inhomogeneous System 32

6.2.1	Constant \bar{V}	32
6.2.2	Function $\bar{V}(\rho)$	33
6.3	The Similarity Solution	34
7	Conclusions and Further Work	37

Chapter 1

Introduction

Much interest has been focused on traffic flow models over the last few decades as the amount of traffic on the roads continues to increase. Congestion is becoming more of a problem and as a consequence the accident rate is also increasing. Today there exist many schemes which not only aim to safely control the traffic but also to maximise its flow. Consider, for example, the variable speed limits on motorways. Information of the amount of vehicles and the traffic conditions on the road is recorded and the speed restrictions altered accordingly. Such schemes depend on the realistic modelling of the flow of traffic, given certain road conditions, in order to accurately predict the behaviour of the traffic over time.

Similarities can be drawn between the flow of traffic and that of a shallow fluid and as such many models have been based on the shallow water equations. Chapter 2 describes some of these models and outlines the drawbacks of such an assumption. Furthermore, we see in Section 3.1 that granular avalanche flow can be described by similar means, and we can apply some of the techniques involved in this field to our traffic model. Chapter 2 continues with the derivation of the continuum BMW [5] model from the car-following Bando [1] model.

In Chapter 3 we derive an alternative continuum model and, by introducing a moving coordinated system, we find a similarity solution to the system.

The behaviour of this solution, as time increases, is discussed and we later use this information as a comparison to our numerical scheme.

In Chapter 4 we consider the homogeneous system. Given sets of initial data with a single discontinuity we solve the Riemann problem of the homogeneous system to determine the behaviour and type of discontinuity.

Chapter 5 develops the First Order Upwind Scheme with Roe decomposition and we use the results of the Riemann problem to compare the programs output for the homogeneous system. The results for the homogeneous system and the inhomogeneous system, including the similarity solution, follows in Chapter 6.

Lastly, we draw conclusions on the method from the numerical results and suggest improvements and areas of further study.

Throughout the text we take the word *car* to be synonymous with *vehicle*.

Chapter 2

Traffic Models

There are two main techniques used to describe the flow of traffic; *microscopic* models and *macroscopic* models. Section 2.1 gives an overview of the microscopic approach, in particular the Bando [1] model. Section 2.2 is concerned with macroscopic methods and the derivation of the Berg, Mason and Woods [5] model from the Bando model.

2.1 Microscopic Models

The Car-Following, or microscopic methods, are a car-by-car Lagrangian like approach. In effect, we consider the traffic as seen from a moving vehicle. These methods consider each vehicle separately and model its behaviour as it reacts to vehicles in front. Traffic flow is *anisotropic*, that is each car reacts to only those in front. The velocity of each vehicle is modelled by an ordinary differential equation dependent on its velocity and headway, where headway is *the distance between the front of the vehicle and the front of the preceding vehicle*. Since this method generates as many ordinary differential equations as the number of vehicles in the system, this number must be small enough in order for the solution of the system to be computationally feasible.

2.1.1 The Bando Model

In 1995 Bando *et al.* [1] published a paper on *The Dynamical Model of Traffic Congestion and Numerical Simulation* which aims to model the “*dynamical evolution of congestion*”. Here they refer to a type of congestion caused by a small perturbation in the initial data rather than a specific source. In other words, they are not concerned with congestion caused by familiar occurrences such as a road accident or traffic lights changing.

Firstly they make the assumption that each vehicle travels at a certain *legal velocity* which is dependent on the headway b . An alternative assumption, often made in earlier models, is that a vehicle must keep a safe legal distance between itself and the car in front. These assumptions are made so that the vehicles avoid traffic accidents.

Bando *et al.* propose the following model for the acceleration of a car at $x = x_n$

$$\ddot{x}_n = a(V(\Delta x_n) - \dot{x}_n), \quad (2.1)$$

where $\dot{x}_n(t)$ is the velocity and V is the *optimal legal velocity*, of car n , dependent on the headway $b_n = \Delta x_n = x_{n+1} - x_n$. The relaxation constant a represents the driver’s sensitivity, defined as the inverse of the driver’s reaction time. They assume that each driver has the same sensitivity and leave as further work the situation where a_n is individual to each driver, and possibly dependent on \dot{x} or b as well. Without loss of generality they set $a = 1$. The model describes the acceleration and deceleration of a vehicle as its headway increases or decreases respectively. However, a vehicle cannot accelerate to a velocity greater than V , which is monotonically increasing and bounded above.

Two models are discussed; a simple model where

$$V(b_n) = \tanh(b) \quad (2.2)$$

and a realistic model where

$$V(\Delta x) = V(b_n) = \tanh(b_n - 2) - \tanh(-2). \quad (2.3)$$

Both models are studied with the initial data $L = 200$ and $N = 100$ where L is the length of the circuit (assuming periodic boundary conditions) and N is the number of cars on the road, and $b = \frac{L}{N}$. This initial data produces a stable model. The conditions for stability are analysed in [1]. A small perturbation is introduced in the movement of the first vehicle and the solution is advanced with time. The model with the optimal velocity function (2.3) generates spontaneous congestion and appears to realistically describe actual traffic.

2.2 Macroscopic Models

Alternative models come from a continuum or macroscopic approach which is an Eulerian, fluid-like approach. These models describe the average velocity and density of the traffic at a point. Unlike the car-following method the movement of all the vehicles is described by two coupled partial differential equations (except for the LWR model, see below), and is therefore less computationally expensive to solve.

All continuum models consist of a conservation equation, namely

$$\rho_t + (\rho v)_x = 0, \tag{2.4}$$

where $v(x, t)$ is the velocity. The density $\rho(x, t)$ of the traffic is the mass of vehicles per kilometre at time t . This conservation equation conserves the mass of vehicles in the system which is dependent on the flow (flux) of cars entering, leaving and already in the system. It amounts to saying that vehicles cannot appear or disappear. The conservation of mass equation is then coupled with a second conservation of momentum equation (or dynamic equation) dependent on the characteristics of the traffic. The non-linearity of such a system automatically generates congestion given smooth initial data.

There are many macroscopic models that have been developed over the last fifty years. In 1955 Lighthill and Whitham published two papers on kinematic waves. The latter paper [2] models the traffic solely by the conservation law (2.4) where the velocity v is assumed to be a decreasing function of the

density ρ . In the following year a similar paper was published by Richards independent of Lighthill and Whitham, and the single equation model,

$$\rho_t + (\rho V(\rho))_x = 0,$$

is known as the LWR model. Zhang [6], who gives a clear introduction to macroscopic modelling, states that the LWR model is capable of describing some features of traffic such as vehicles approaching and leaving traffic congestion where a *shock* forms, and the anisotropic nature of real traffic. However, due to certain assumptions, the LWR model is incapable of describing other aspects of traffic flow, in particular flow through narrow spaces (bottlenecks) or when the traffic stops and starts.

In the 1970s Payne and Whitham [3] developed a different approach to the macroscopic model. They drew similarities between the flow of traffic and fluid and based their model on the Navier-Stokes equations of incompressible flow. The PW model is

$$v_t + vv_x = \frac{V(\rho) - v}{\tau} - \frac{c(\rho)}{\rho} \rho_x \quad (2.5)$$

where τ , the relaxation term, is the driver's reaction time, $V(\rho)$ is a velocity function of the density and $c(\rho)$ is an anticipation term as described in [8]. However, the PW model can give negative speeds allowing the cars to travel backwards. Also the assumption that traffic flow is fluid-like does not agree with the anisotropic nature of physical traffic flow. This is because fluid particles are *isotropic* and as such react equally to information from behind as well as from in front.

The following years saw several attempts to improve the PW model. Modifications have been made by, amongst others, Kerner and Konhäuser [4] who included a viscosity term to stop the formation of unrealistic shocks,

$$v_t + vv_x = \frac{V(\rho) - v}{\tau} - \frac{c_0^2}{\rho} \rho_x + \mu \frac{v_{xx}}{\rho}, \quad (2.6)$$

and Zhang who replaced the constant, c_0^2 in (2.6) with the function $c(\rho)$ in order to solve the problem of negative velocities. These models all yield some

unrealistic traffic properties due to the close link with fluid flow. Aw and Rascle [7] develop a different second equation, Lagrangian in nature, in an attempt to overcome this problem.

2.2.1 The BMW Model

In 2000 Berg, Mason and Woods [5] (BMW) proposed a continuum model derived from the Bando car-following model (2.1) written in terms of the density ρ rather than the headway b . Usually the density is defined as

$$\rho = \frac{1}{b}. \quad (2.7)$$

Berg *et al.*, however, state that this definition is inaccurate. They consider the open interval $(1, y)$ with cars at positions $x = 1, 2, 4, 8, \dots, n, \dots$ so the car at the point x has a headway $b = x$.

Assuming that (2.7) holds, $\rho = \frac{1}{x}$ and thus the number of cars in the open interval $(1, y)$ is

$$\int_1^y \frac{1}{x} dx = \log_e y. \quad (2.8)$$

From the above diagram we see that the headway of car n is $b = y = 2^n$. Therefore, the number of cars in the interval is $n = \log_2 y$. Hence the assumption that $\rho = \frac{1}{b}$ is, in fact, incorrect by a factor of $\log_e 2$. As illustrated below, Berg *et al.* find an alternative definition relating the density to the headway by calculating a higher order approximation to $\rho(b)$.

Berg *et al.* state that a more accurate relation between ρ and b is

$$\int_{x_n}^{x_n+b} \rho(x, t) dx = 1,$$

for all i where x_i is the position of car i at a given time. They set up a consistent mapping between the positions of the vehicles, $\{x_i\}$, and their associated density function, $\rho(x)$. This mapping is not unique. However, given the position of the first car the inverse mapping is unique and it is this which is required to derive a macroscopic momentum equation from (2.1).

Considering all cars on a road, Berg *et al.* expand (2.8) as

$$\int_x^{x+b(x,t)} \rho(x', t) dx' = \int_0^b \rho(x+y, t) dy \equiv 1 \quad (2.9)$$

using the change of variable $x' = x + y$. This is expanded in powers of y giving

$$\int_0^{b(x,t)} \left(\rho + y\rho_x + \frac{y^2\rho_{xx}}{2!} + \dots \right) dy = 1,$$

and integrating,

$$b\rho + \frac{b^2\rho_x}{2!} + \frac{b^3\rho_{xx}}{3!} + \dots = 1. \quad (2.10)$$

The series is expanded to this order so as to produce a macroscopic model that describes the desired traffic attributes and keeps the same stability criterion as (2.1). The stability of the BMW model is analysed clearly in [5]. Since (2.10) is an asymptotic series the cubic term is small compared to the preceding terms and Berg *et al.* seek an initial approximation to a solution of the quadratic

$$b\rho + \frac{b^2\rho_x}{2} \approx 1 \quad (2.11)$$

to the same order, in small quantities, by setting $b \approx \frac{1}{\rho} + A\rho_x$ giving

$$\left(\frac{1}{\rho} + A\rho_x \right) \rho + \frac{1}{2!} \left(\frac{1}{\rho} + A\rho_x \right)^2 \rho_x \approx 1.$$

Solving this quadratic

$$b \approx \frac{1}{\rho} - \frac{\rho_x}{2\rho^3}.$$

This is extended further, as a perturbation series, using (2.10) in the form

$$b = -\frac{1}{\rho} \left(\frac{b^2\rho_x}{2!} + \frac{b^3\rho_{xx}}{3!} + \dots \right)$$

and substituting in (3.8) to give

$$b \approx \frac{1}{\rho} - \frac{\rho_x}{2\rho^3} - \frac{\rho_{xx}}{6\rho^4} + \frac{\rho_x^2}{2\rho^5} \quad (2.12)$$

as an approximation to the headway in terms of the density.

Taking the derivative of (2.9) using Leibnitz's Rule gives the conservation equation (2.4) and hence v is consistent in the model. Equation (2.12) is then applied to the Bando model (2.1) using

$$\begin{aligned} V_B(b_n) &= V_B\left(\frac{1}{\rho} - \frac{\rho_x}{2\rho^3} - \frac{\rho_{xx}}{6\rho^4} + \frac{\rho_x^2}{2\rho^5}\right) \\ &= V_B\left(\frac{1}{\rho}\right) + \left(-\frac{\rho_x}{2\rho^3} - \frac{\rho_{xx}}{6\rho^4} + \frac{\rho_x^2}{2\rho^5}\right) V_B'\left(\frac{1}{\rho}\right) \\ &= \bar{V}(\rho) + \bar{V}'(\rho) \left(\frac{\rho_x}{2\rho} + \frac{\rho_{xx}}{6\rho^2} - \frac{\rho_x^2}{2\rho^3}\right), \end{aligned}$$

where $\bar{V}(\rho) = V_B\left(\frac{1}{\rho}\right)$ which gives a second dynamic equation of type (2.1) in the form

$$v_t + vv_x = a[\bar{V}(\rho) - v] + a\bar{V}'(\rho) \left[\frac{\rho_x}{2\rho} + \frac{\rho_{xx}}{6\rho^2} - \frac{\rho_x^2}{2\rho^3}\right], \quad (2.13)$$

to be coupled with (2.4). Here the pressure-like term ρ_x (cf. gas kinetics) causes the traffic flow to become unstable and so the diffusive term ρ_{xx} is included to cancel its effects and smooth traffic density. The accuracy will increase if further terms of the asymptotic series are included in the derivation of ρ .

Setting $a = \frac{1}{\tau}$ the BMW model is analogous to the Kerner and Konhäuser model (2.6) where $-\frac{\bar{V}'(\rho)}{2}$ is analogous to c_0^2 and the coefficients of the higher order terms are assumed to be dependent on ρ rather than constant. Berg *et al.* compare their model with numerical simulations of the Bando equation (2.1) which show these coefficients (2.13) must depend on ρ in order for the shock wave solutions to agree. They state that, under certain circumstances, traffic shocks are modelled well by travelling waves using the continuum model. It has also been shown in [8] that the BMW gives reasonably good results for modelling traffic flow.

This chapter has given a brief insight to the car-following and continuum methods of traffic modelling and, in particular, the derivation of the BMW model from the Bando model. In the next chapter we discuss a limitation in this derivation and consider a new conservation of momentum equation also based on the Bando model.

Chapter 3

A New Macroscopic Model

One criticism with the BMW model is that there exists some weakness in its derivation if it is to be applied at shocks. Equation (2.10) is assumed to be an asymptotic series. That is, each term is of a smaller magnitude than the preceding term. However, if the model is applied at a discontinuity where the density ρ changes rapidly, the equation will not be a valid asymptotic series. We, therefore, aim to develop an alternative system which is also derived from the microscopic Bando model.

We make the assumptions that a driver wishes to travel at the optimal velocity \bar{V} but to accelerate if b_x , the change in the headway, is positive and decelerate if b_x is negative. As such, an extra term is added the Bando car-following model giving a new dynamic equation

$$v_t + vv_x = a(\bar{V}(\rho) - v) + Cb_x, \quad (3.1)$$

where C is a positive constant which governs the effect b_x has on the equation. As with all continuum models this is coupled with a conservation of mass equation, namely (2.4), to give

$$\begin{aligned} \rho_t + (\rho v)_x &= 0 \\ v_t + vv_x &= a(\bar{V}(\rho) - v) + Cb_x. \end{aligned} \quad (3.2)$$

In Chapter 5 we model the solution of the system with a numerical scheme. However, we first seek an exact solution to compare with the results of the numerical scheme.

3.1 A Similarity Solution

In 2001 Tai *et al.* [10] published a paper concerned with the modelling of granular avalanche flow. They consider a granular material of finite mass moving along a flat surface and, by the introduction of a moving coordinate system they find a similarity solution to their problem. It is this method of change of variables that we implement here to find a similarity solution to the new macroscopic system (3.2)

$$\begin{aligned}\rho_t + (\rho v)_x &= 0 \\ v_t + vv_x &= a(\bar{V} - v) + Cb_x,\end{aligned}\tag{3.3}$$

where the optimal velocity \bar{V} is assumed to be constant.

We set $v = v_0 + \check{v}$, where \check{v} is a relative velocity and v_0 is a base velocity which satisfies

$$v_{0t} = (\bar{V} - v_0).$$

Now v_0 can be found by solving

$$\int \frac{dv_0}{\bar{V} - v_0} = \int a dt$$

with the initial condition $v_0(0) = 0$ giving

$$v_0 = \bar{V}(1 - e^{-at}).$$

We change the variables of the system from x and t to ξ and τ using the transformation

$$\xi = x - \int_0^t v_0(t') dt'.\tag{3.4}$$

Applying this to the conservation of mass equation gives

$$\frac{\partial \rho}{\partial \tau} \frac{\partial \tau}{\partial t} + \frac{\partial \rho}{\partial \xi} \frac{\partial \xi}{\partial t} + \frac{\partial(\rho v)}{\partial \tau} \frac{\partial \tau}{\partial x} + \frac{\partial(\rho v)}{\partial \xi} \frac{\partial \xi}{\partial x} = 0$$

where $\frac{\partial \tau}{\partial t} = 1$, $\frac{\partial \xi}{\partial t} = -v_0$, $\frac{\partial \tau}{\partial x} = 0$ and hence

$$\frac{\partial \rho}{\partial \tau} - v_0 \frac{\partial \rho}{\partial \xi} + \frac{\partial(\rho v)}{\partial \xi} = 0.$$

Substituting for v and replacing τ with t

$$\frac{\partial \rho}{\partial t} - v_0 \frac{\partial \rho}{\partial \xi} + \frac{\partial(\rho \check{v})}{\partial \xi} + \frac{\partial(\rho v_0)}{\partial \xi} = 0$$

which reduces to

$$\frac{\partial \rho}{\partial t} + \frac{\partial(\rho \check{v})}{\partial \xi} = 0 \quad (3.5)$$

since v_0 does not depend on ξ .

We substitute for v in the second equation (3.2) of the system to give

$$\check{v}_t + v_{0t} + vv_x + v_0 \check{v}_x = a(\bar{V} - \check{v} - v_0)$$

and, using the relation for v_{0t} above, this reduces to

$$\check{v}_t + \check{v}\check{v}_x + v_0 \check{v}_x = -a\check{v} + Cb_x.$$

After applying the transformation of variables (3.4)

$$\frac{\partial \check{v}}{\partial \tau} - \frac{\partial \check{v}}{\partial \xi} v_0 + \check{v} \frac{\partial \check{v}}{\partial \xi} + v_0 \frac{\partial \check{v}}{\partial \xi} = -a\check{v} + C \frac{\partial b}{\partial \xi}$$

and, again setting $\tau = t$,

$$\frac{\partial \check{v}}{\partial t} + \check{v} \frac{\partial \check{v}}{\partial \xi} - C \frac{\partial b}{\partial \xi} + a\check{v} = 0. \quad (3.6)$$

To obtain a similarity solution we suppose that \check{v} varies linearly with ξ , i.e. $\check{v} = \xi f(t)$ and as such (3.6) becomes

$$\xi f' + \xi f^2 - C \frac{\partial b}{\partial \xi} + a\xi f = 0. \quad (3.7)$$

We then find an expression for the headway b by integrating the above with respect to ξ and, with the initial condition $b = b_0(t)$ when $\xi = 0$,

$$\frac{\xi^2}{2} (f' + f^2 + af) - Cb = Cb_0(t).$$

This is rearranged to give

$$b = \frac{\xi^2}{2C} (f' + f^2 + af) + b_0(t). \quad (3.8)$$

Recall the conservation of mass equation after the change of variables
(3.5)

$$\frac{\partial \rho}{\partial t} + \frac{\partial(\rho \check{v})}{\partial \xi} = 0.$$

We replace ρ by $\frac{1}{b}$ giving

$$\frac{\partial b}{\partial t} - b \frac{\partial \check{v}}{\partial \xi} + \check{v} \frac{\partial b}{\partial \xi} = 0 \quad (3.9)$$

and then substituting in for b , given in (3.8), where

$$\frac{\partial b}{\partial t} = \frac{\xi^2}{2C}(f' + f^2 + af)' + b'_0$$

and

$$\frac{\partial b}{\partial \xi} = \frac{\xi}{C}(f' + f^2 + af),$$

we next make our substitution for \check{v} to obtain (3.9) in the form

$$\frac{\xi^2}{2C}(f' + f^2 + af)' + b'_0 + \frac{f\xi^2}{2C}(f' + f^2 + af) - fb_0 = 0.$$

This holds for all ξ if

$$b'_0 = fb_0 \quad (3.10)$$

and

$$(f' + f^2 + af)' = -f(f' + f^2 + af) \quad (3.11)$$

Rewriting equation (3.10) in terms of ρ_0 where $b_0 = \frac{1}{\rho_0}$ gives

$$\rho'_0 = -f\rho_0 \quad (3.12)$$

which we substitute into (3.11) and integrating with respect to t , we arrive at

$$f' = A\rho_0 - f^2 - af \quad (3.13)$$

where A is a positive constant of integration. This system of two ordinary differential equations has a fixed point at $(\rho, f) = (0, 0)$. We plot ρ_0 against f to investigate their behaviour as time $t \rightarrow \infty$. Hence we can deduce the behaviour of the system as time evolves.

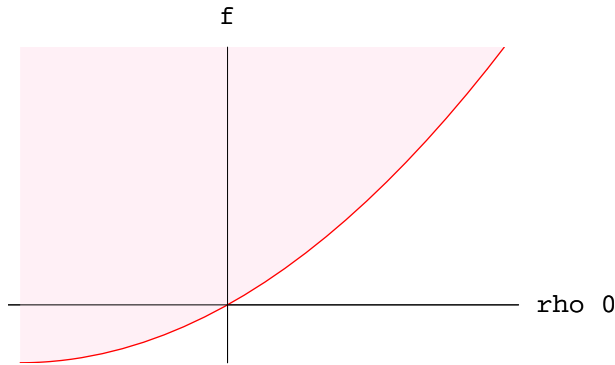


Figure 3.1: Plot of $f' = \frac{A}{\rho_0} - f^2 - af = 0$. The shaded region indicates where $f' < 0$.

Since both f and ρ_0 are positive ρ_0' is always negative. The shaded area in Figure 3.1 indicates the region where $f' < 0$. Given any initial point within this region, the solution will tend towards the fixed point as $t \rightarrow \infty$. This is easily seen for small initial values of f . However, if f is large in comparison to ρ_0 the gradient of the solution is steep and in time will cross the curve where $f' = 0$ into the region where $f' > 0$. At this point its gradient becomes positive and it will cross the curve again. The curve $f' = 0$ is an attractor and as such any solution in the shaded region will tend to the fixed point. Moreover, any initial point will also tend to this fixed point. As $t \rightarrow \infty$ both $f \rightarrow 0$ and $\rho_0 \rightarrow 0$ and so $v = (v_0 + \check{v}) \rightarrow \bar{V}$ the optimal velocity. These findings are later compared to the solution of the numerical scheme for the similarity solution.

Having investigated the behaviour of a similarity solution to the inhomogeneous system, we now consider an analytic solution of the homogeneous system.

Chapter 4

The Homogeneous System

In this chapter we look at the case when $a = 0$. This homogeneous sub-problem of (3.2) is

$$\begin{aligned} \rho_t + (\rho v)_x &= 0 \\ v_t + vv_x &= Cb_x \end{aligned}, \tag{4.1}$$

where the zero relaxation term a means there is no source term $(\bar{V} - v)$. In Section 4.1 we find a solution to a Riemann problem of the system. In order to do this we start by writing the system in *conservation form*

$$\mathbf{u}_t + \mathbf{f}(\mathbf{u})_x = \mathbf{R}(\mathbf{u}).$$

In Chapter 5 we require the full inhomogeneous system in conservation form, consequently we shall consider (3.2) here and substitute in $a = 0$ later to give the homogeneous case.

We multiply the conservation of mass equation by v , the inhomogeneous, dynamic equation (3.1) by ρ and using the product rule of partial differentiation

$$v\rho_t + v^2\rho_x + \rho vv_x = 0 \tag{4.2}$$

and

$$\rho v_t + \rho vv_x = \rho a(\bar{V} - v) + \rho Cb_x. \tag{4.3}$$

Adding these two equations,

$$v\rho_t + \rho v_t + v^2\rho_x + 2\rho vv_x = \rho a(\bar{V} - v) + \rho Cb_x$$

and simplifying, we obtain

$$(\rho v)_t + (\rho v^2)_x = \rho a(\bar{V}(\rho) - v) + \rho C b_x.$$

We now assume that the usual relation between the density and the headway holds, i.e. $b = \frac{1}{\rho}$. Therefore, $b_x = -\frac{\rho_x}{\rho^2}$ and so $\rho b_x = (\ln \rho)_x$. Substituting this into the above gives

$$(\rho v)_t + (\rho v^2)_x + C(\ln \rho)_x = \rho a(\bar{V}(\rho) - v)$$

which is our dynamic equation where the left hand side is in conservation form and the right hand side is a source term. We write the system in vector form as

$$\begin{pmatrix} \rho \\ \rho v \end{pmatrix}_t + \begin{pmatrix} \rho v \\ \frac{(\rho v)^2}{\rho} + C \ln \rho \end{pmatrix}_x = \begin{pmatrix} 0 \\ a\rho(\bar{V}(\rho) - v) \end{pmatrix}.$$

The solution of the system consists of two waves travelling in different directions. To find the speeds of these waves we next write the system in *quasi-linear* form

$$\frac{\partial \mathbf{u}}{\partial t} + \frac{\partial \mathbf{f}}{\partial \mathbf{u}} \mathbf{u}_x = \mathbf{R}(\mathbf{u})$$

where

$$\mathbf{A} = \frac{\partial \mathbf{f}}{\partial \mathbf{u}} = \begin{pmatrix} 0 & 1 \\ \frac{C}{\rho} - v^2 & 2v \end{pmatrix}. \quad (4.4)$$

The wave speeds are given by the eigenvalues of the Jacobian matrix \mathbf{A} . These are found by solving the characteristic equation of \mathbf{A}

$$|A - \lambda I| = 0,$$

giving eigenvalues

$$\lambda_1 = v - \sqrt{\frac{C}{\rho}}, \quad \lambda_2 = v + \sqrt{\frac{C}{\rho}}$$

and corresponding eigenvectors

$$\mathbf{r}_1 = \begin{pmatrix} 1 \\ v - \sqrt{\frac{C}{\rho}} \end{pmatrix}, \quad \mathbf{r}_2 = \begin{pmatrix} 1 \\ v + \sqrt{\frac{C}{\rho}} \end{pmatrix}$$

such that $(\mathbf{A} - \lambda_k I)\mathbf{r}_k = 0$, for $k = 1, 2$. The system is non-linear and, in general, an analytic solution of such is not possible. However, we can find an exact solution of the Riemann problem, consisting of initial data giving a single discontinuity between two constant states.

4.1 The Riemann Solution

We now consider the non-linear, homogeneous system (4.1) which gives $\mathbf{R} = 0$ in the conservation form. The eigenvalues are real and distinct thus ensuring *strict hyperbolicity*.

Given the initial data at time $t = 0$

$$\mathbf{u} = \begin{cases} \mathbf{u}_L & x \leq 0 \\ \mathbf{u}_R & x \geq 0 \end{cases}$$

there is a discontinuity at the origin. We decompose the initial discontinuity into n (here $n = 2$) separate waves between $n + 1$ constant states. Each new k -wave, with $k = 1, \dots, n$ is one of the following three types of discontinuity.

Hugoniot Curve This is a *genuinely non-linear* discontinuity with shock speed s . It satisfies both the jump condition and the entropy condition (given below). The characteristic go into the shock.

Contact Discontinuity These are discontinuities of linearly degenerate fields. Here the characteristics are parallel to the discontinuity.

Rarefaction This is a simple wave solution joining two constant states.

The k -Riemann invariants are constant on the characteristics.

The solution is then constructed in phase space by linking the constant end states \mathbf{u}_L and \mathbf{u}_R by a path of valid waves via the intermediate states.

We consider our non-linear, homogeneous system (4.1) in conservation form with initial data

$$\mathbf{u}_L = \begin{pmatrix} \rho_L \\ (\rho v)_L \end{pmatrix} = \begin{pmatrix} 0.2 \\ 0.12 \end{pmatrix}$$

$$\mathbf{u}_R = \begin{pmatrix} \rho_R \\ (\rho v)_R \end{pmatrix} = \begin{pmatrix} 0.6 \\ 0.09 \end{pmatrix}$$

where $0 \leq x \leq 30$ so the discontinuity lies at $x = 15$. This initial data is used in [8] to test the Riemann problem for the PW, Zhang and Aw and Rascle models. Here we have normalised ρ and v such that $\rho \in [0, 1]$ and $v \in [0, 1]$. The initial data models a situation where traffic travels from low density to high density, for example when approaching congestion.

The Rankine-Hugoniot jump condition is

$$\mathbf{f}(\mathbf{u}) - \mathbf{f}(\hat{\mathbf{u}}) = s(\mathbf{u} - \hat{\mathbf{u}}),$$

where the fixed state $\hat{\mathbf{u}}$ is either \mathbf{u}_L or \mathbf{u}_R , \mathbf{f} is the flux and s is the shock speed. Applying this to our system yields the two equations

$$\begin{aligned} \rho v - \hat{\rho} \hat{v} &= s(\rho - \hat{\rho}) \\ \rho v^2 + C \ln \rho - \hat{\rho} \hat{v}^2 - C \ln \hat{\rho} &= s(\rho v - \hat{\rho} \hat{v}), \end{aligned}$$

giving shock speeds

$$s = \frac{\rho v - \hat{\rho} \hat{v}}{\rho - \hat{\rho}},$$

where v is given by solving the quadratic

$$(\rho v - \hat{\rho} \hat{v})^2 - (\rho v^2 + C \ln \rho - \hat{\rho} \hat{v}^2 - C \ln \hat{\rho})(\rho - \hat{\rho}) = 0.$$

Hence,

$$v = \hat{v}_-^+ \sqrt{\frac{C(\ln \rho - \ln \hat{\rho})(\rho - \hat{\rho})}{\rho \hat{\rho}}} \quad (4.5)$$

gives the Hugoniot curves. Figures 4.1 and 4.2 show plots of v at $\hat{\mathbf{u}} = \mathbf{u}_L$ and $\hat{\mathbf{u}} = \mathbf{u}_R$ where the green lines represent $v = \hat{v} - \sqrt{\frac{C(\ln \rho - \ln \hat{\rho})(\rho - \hat{\rho})}{\rho \hat{\rho}}}$ and the blue lines where v takes the positive sign. We see that if either sign is chosen for all ρ , then v is not a smooth curve as one would expect. In fact, v switches between the two Hugoniot curves at $\hat{\mathbf{u}}$. The modified equation

$$v = \hat{v}_-^+ \operatorname{sgn}(\rho - \hat{\rho}) \sqrt{\frac{C(\ln \rho - \ln \hat{\rho})(\rho - \hat{\rho})}{\rho \hat{\rho}}} \quad (4.6)$$

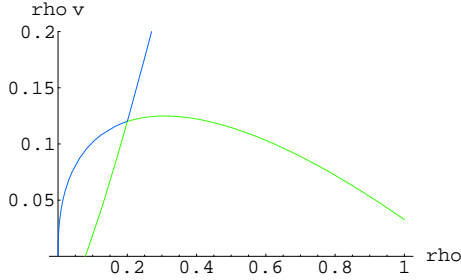


Figure 4.1: *The two curves given by (4.5) through \mathbf{u}_L .*

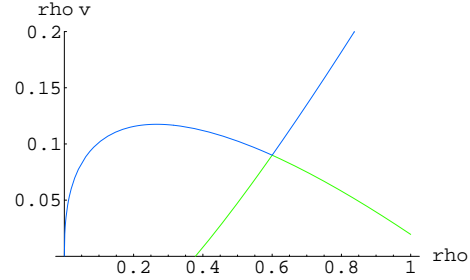


Figure 4.2: *The two curves given by (4.5) through \mathbf{u}_R .*

will, therefore, ensure smooth Hugoniot curves by selecting the correct sign.

At each state, \mathbf{u}_L or \mathbf{u}_R , there are two possible Hugoniot curves. We require the k -Hugoniot curve, v_k , that is tangent to the k -eigenvector, r_k , at $\hat{\mathbf{u}}$. Figures 4.3 and 4.4 show the two possible smooth Hugoniot curves and the eigenvector, \mathbf{r}_k , at each end state $\hat{\mathbf{u}}$. The red lines show the eigenvector, \mathbf{r}_k , the green and blue lines show the Hugoniot curves where v takes the negative and positive signs respectively.

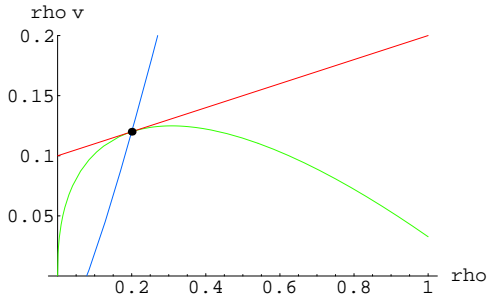


Figure 4.3: *The solid green line indicates the correct 1-Hugoniot curve which is tangent to the 1-eigenvector at \mathbf{u}_L .*

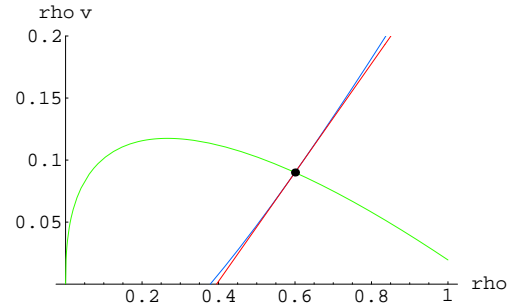


Figure 4.4: *The solid blue line indicates the correct 2-Hugoniot curve which is tangent to the 2-eigenvector at \mathbf{u}_R .*

The 1-Hugoniot curve at \mathbf{u}_L is

$$v_1 = \hat{v} - \text{sgn}(\rho - \hat{\rho}) \sqrt{\frac{C(\ln \rho - \ln \hat{\rho})(\rho - \hat{\rho})}{\rho \hat{\rho}}}$$

and at \mathbf{u}_R the 2-Hugoniot curve is

$$v_2 = \hat{v} - \text{sgn}(\rho - \hat{\rho}) \sqrt{\frac{C(\ln \rho - \ln \hat{\rho})(\rho - \hat{\rho})}{\rho \hat{\rho}}}.$$

Since the two states do not lie on the same Hugoniot curve the discontinuity is not a single shock, but rather the end states \mathbf{u}_L and \mathbf{u}_R are connected by valid waves via \mathbf{u}_M some intermediate state. In order for the Hugoniot curves to be valid we require the k -characteristic fields to be genuinely non-linear, that is

$$(\nabla_{\mathbf{u}} \lambda_k) \cdot \mathbf{r}_k(\mathbf{u}) \neq 0$$

for all \mathbf{u} . The system yields

$$(\nabla_{\mathbf{u}} \lambda_1) \cdot \mathbf{r}_1(\mathbf{u}) = \left(\frac{1}{2} \sqrt{\frac{C}{\rho^3}} \quad \frac{1}{\rho} \right) \cdot \left(1 \quad v - \sqrt{\frac{C}{\rho}} \right)^T = -\frac{1}{2} \sqrt{\frac{C}{\rho^3}}.$$

Similarly

$$(\nabla_{\mathbf{u}} \lambda_2) \cdot \mathbf{r}_2(\mathbf{u}) = \frac{1}{2} \sqrt{\frac{C}{\rho^3}}$$

and hence it is genuinely non-linear. Incidentally, if $(\nabla_{\mathbf{u}} \lambda_k) \cdot \mathbf{r}_k(\mathbf{u}) = 0$ then we have a contact discontinuity. We now calculate where the Hugoniot curves are valid by using Lax's entropy condition at each constant end state

$$\lambda_1(\mathbf{u}_L) > s > \lambda_1(\mathbf{u}) \quad \text{and} \quad \lambda_2(\mathbf{u}_R) < s < \lambda_2(\mathbf{u})$$

which holds for hyperbolic, genuinely non-linear conservation laws. Figures 4.5 and 4.6 are plots of $\lambda_k(\hat{\mathbf{u}})$ (in red), s (in green) and $\lambda_k(\mathbf{u})$ (in blue). Figure 4.5 shows the 1-shock is entropy violating to the left of \mathbf{u}_L , where the lines are dashed, and a valid shock to the right where the lines are solid. Figure 4.6 shows a similar situation for 2-shock at \mathbf{u}_R .

We also find the k -Riemann invariants and thus the rarefactions/ simple waves at $\hat{\mathbf{u}}$. The k -Riemann invariants are smooth functions $w_k(\mathbf{u})$ such that

$$\nabla_{\mathbf{u}} w_k(\mathbf{u}) \cdot \mathbf{r}_k = 0$$

giving for the 1-shock

$$\frac{\partial w_1}{\partial(\rho v)} + \frac{\partial w_2}{\partial(\rho v)} \left(v - \sqrt{\frac{C}{\rho}} \right) = 0. \quad (4.7)$$

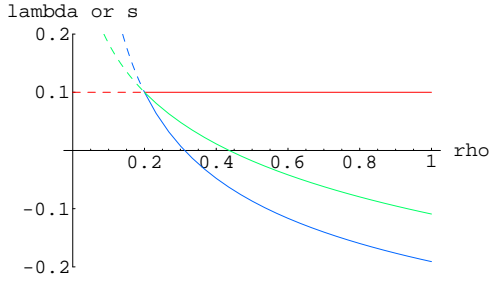


Figure 4.5: *The entropy condition holds to the right of \mathbf{u}_L*

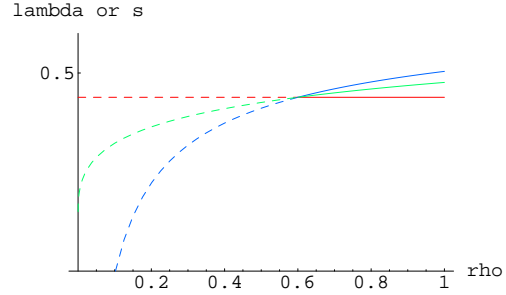


Figure 4.6: *The entropy condition holds to the right of \mathbf{u}_R*

We seek solutions of (4.7) such that w_1 is constant on the characteristics, i.e.

$$\frac{d(\rho v)}{d\rho} - \frac{\rho v}{\rho} + \sqrt{\frac{C}{\rho}} = 0.$$

This is solved using the integrating factor $e^{\int \frac{1}{\rho} d\rho} = \frac{1}{\rho}$, to give the 1-Riemann invariant

$$w_1 = v - 2\sqrt{\frac{C}{\rho}}.$$

We can solve for v by setting

$$w_1 = v - 2\sqrt{\frac{C}{\rho}} = \text{constant} = \hat{v} - 2\sqrt{\frac{C}{\hat{\rho}}}$$

which gives v at \mathbf{u}_L as

$$v_{w1} = \lambda_1(\mathbf{u}_L) + 2\sqrt{\frac{C}{\rho}}.$$

Similarly the 2-Riemann invariant is

$$w_2 = v + 2\sqrt{\frac{C}{\rho}}$$

and v at \mathbf{u}_R is given by

$$v_{w2} = \lambda_2(\mathbf{u}_R) - 2\sqrt{\frac{C}{\rho}}.$$

In the figures below the rarefactions are represented by dashed curves and the shocks by solid curves. The 1-shock and v_{w1} are in green and the 2-shock and v_{w2} are in blue. The black points give the end states. Figure 4.9 shows the admissible rarefactions, given by v_{wk} , and shocks, v_k , and where they cross at \mathbf{u}_M the red point. Figure 4.10 is an enlargement of the region containing \mathbf{u}_M and \mathbf{u}_L where Mathematica finds $\mathbf{u}_M = (0.62 \ 0.10)^T$. The left hand state \mathbf{u}_L is connected to the right hand state, \mathbf{u}_R by two Hugoniot curves which intersect at \mathbf{u}_M .

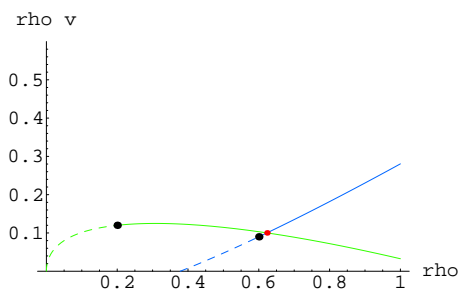


Figure 4.7: *The intersection of the valid Hugoniot curves and rarefaction waves connecting \mathbf{u}_L to \mathbf{u}_R via \mathbf{u}_M .*

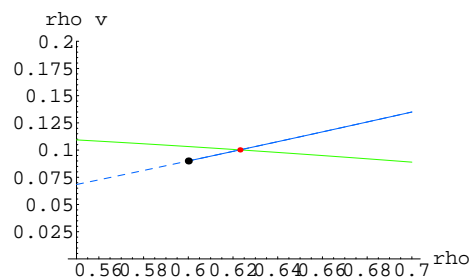


Figure 4.8: *Close up of the intersection at \mathbf{u}_M .*

4.1.1 Different Initial Data

We consider the situation where traffic moves away from congestion and high density towards lower density, for example when leaving a traffic jam or as traffic lights turn green. This circumstance uses the initial data where \mathbf{u}_L and \mathbf{u}_R are reversed, and so

$$\mathbf{u}_L = \begin{pmatrix} \rho_L \\ (\rho v)_L \end{pmatrix} = \begin{pmatrix} 0.6 \\ 0.09 \end{pmatrix} \quad \text{and} \quad \mathbf{u}_R = \begin{pmatrix} \rho_R \\ (\rho v)_R \end{pmatrix} = \begin{pmatrix} 0.2 \\ 0.12 \end{pmatrix}.$$

The Riemann problem is solved as before but now the end states are connected via two rarefaction waves and $\mathbf{u}_M = (0.195 \ 0.11)^T$ as seen in Figure 4.9.

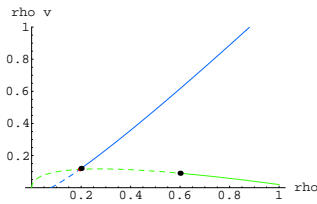


Figure 4.9: *The intersection of the valid Hugoniot curves and rarefaction waves connecting \mathbf{u}_L to \mathbf{u}_R via \mathbf{u}_M .*

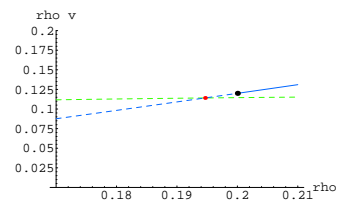


Figure 4.10: *Close up of the intersection at \mathbf{u}_M .*

Chapter 5

The Numerical Method

We have found the Riemann solution to the homogeneous system and also a similarity solution to the inhomogeneous system. We now wish to apply a numerical scheme and compare the results to the analytic solutions. We consider the Roe scheme in Section 5.2 but first we describe the Roe decomposition for the inhomogeneous system.

5.1 Roe Decomposition

In order to write the numerical Roe scheme we first consider the Roe decomposition of the non-linear, homogeneous system (3.2). Roe decomposes the system into scalar problems by locally approximating the Jacobian matrix A as constant over discrete cells.

With the system written in conservation form

$$\begin{pmatrix} \rho \\ \rho v \end{pmatrix}_t + \begin{pmatrix} \rho v \\ \frac{(\rho v)^2}{\rho} + C \ln \rho \end{pmatrix}_x = \begin{pmatrix} 0 \\ a\rho(\bar{V}(\rho) - v) \end{pmatrix}.$$

we seek $\tilde{A}(\mathbf{u})$ such that

$$\tilde{A}\Delta\mathbf{u} = \Delta\mathbf{f}. \tag{5.1}$$

This is the shock capturing property where $\Delta\mathbf{u} = \mathbf{u}_R - \mathbf{u}_L$ is a small difference over an interval (x_L, x_R) and \mathbf{u}_L and \mathbf{u}_R are taken at the left and right ends of the cell respectively.

Recall (4.4) giving the Jacobian matrix A , we set

$$\tilde{A} = \begin{pmatrix} 0 & 1 \\ \frac{C}{\tilde{\rho}} - \tilde{v}^2 & 2\tilde{v} \end{pmatrix}$$

where we assume $\tilde{v}^2 = \tilde{v}^2$ and find expressions for the averages \tilde{v} and $\tilde{\rho}$ in terms of v and ρ . The method considers average values, denoted by tilde, which satisfy the discrete system taken in each cell. These averages are not unique and therefore the above assumption need not hold. It can, however, be shown to be correct for our system. Equation (5.1) then gives

$$\Delta(\rho v) = \Delta(\rho v)$$

and

$$\left(\frac{C}{\tilde{\rho}} - \tilde{v}^2\right) \Delta\rho + 2\tilde{v}\Delta(\rho v) = \Delta(\rho v^2 + C \ln \rho).$$

The second equation holds if

$$\frac{C}{\tilde{\rho}} \Delta\rho = C \Delta(\ln \rho)$$

giving

$$\tilde{\rho} = \frac{\Delta\rho}{\Delta(\ln \rho)},$$

and if

$$\tilde{v}^2 \Delta\rho - 2\tilde{v}\Delta(\rho v) + \Delta(\rho v^2) = 0 \tag{5.2}$$

where

$$\Delta(\rho v) = \bar{\rho}\Delta v - \bar{v}\Delta\rho = \rho_R v_R = \rho_L v_L$$

and $\bar{\rho} = \frac{1}{2}(\rho_L + \rho_R)$. From the above quadratic (5.2)

$$\tilde{v} = \frac{2\Delta(\rho v) \pm \sqrt{4\Delta(\rho v)^2 - 4\Delta(\rho v^2)\Delta\rho}}{\Delta\rho}$$

which reduces to

$$\tilde{v} = \frac{(\rho_R v_R - \rho_L v_L) \pm \sqrt{(\sqrt{\rho_R v_L v_R} - \sqrt{\rho_R v_L v_L})^2}}{(\sqrt{\rho_R} - \sqrt{\rho_L})(\sqrt{\rho_R} + \sqrt{\rho_L})}.$$

Expanding $(\rho_R v_R - \rho_L v_L)$ and taking the negative root we obtain

$$\tilde{v} = \frac{\sqrt{\rho_R} v_R - \sqrt{\rho_L} v_L}{\sqrt{\rho_R} + \sqrt{\rho_L}}.$$

Next we seek the Roe averages $\tilde{\alpha}_k$ and $\tilde{\beta}_k$ where $k = 1, 2$, such that

$$\Delta \mathbf{u} = \sum_{k=1}^2 \tilde{\alpha}_k \tilde{\mathbf{r}}_k \quad \text{and} \quad \Delta \mathbf{f} = \sum_{k=1}^2 \tilde{\alpha}_k \tilde{\lambda}_k \tilde{\mathbf{r}}_k \quad (5.3)$$

and the right hand side vector

$$\mathbf{R}(\mathbf{u}) = \sum_{k=1}^2 \tilde{\beta}_k \mathbf{r}_k \quad (5.4)$$

where

$$\mathbf{R}(\mathbf{u}) = \begin{pmatrix} 0 \\ a\rho(\bar{V}(\rho) - v) \end{pmatrix}$$

and $\lambda_k = \tilde{v}_\pm \sqrt{\frac{C}{\rho}}$ are the eigenvalues and $\mathbf{r}_k = (1, \tilde{\lambda}_k)^T$ are the corresponding eigenvectors. From the first equation of (5.3) we obtain

$$\tilde{\alpha}_1 + \tilde{\alpha}_2 = \Delta \rho$$

and

$$(\tilde{\alpha}_1 + \tilde{\alpha}_2) + (\tilde{\alpha}_2 - \tilde{\alpha}_1) \sqrt{\frac{C}{\rho}} = \Delta \rho v.$$

Therefore, the $\tilde{\alpha}_k$ are

$$\tilde{\alpha}_1 = \frac{\sqrt{\frac{C}{\rho}} \Delta \rho - \bar{\rho} \Delta v}{2\sqrt{\frac{C}{\rho}}} \quad \text{and} \quad \tilde{\alpha}_2 = \frac{\sqrt{\frac{C}{\rho}} \Delta \rho + \bar{\rho} \Delta v}{2\sqrt{\frac{C}{\rho}}} \quad (5.5)$$

and, from (5.4) the $\tilde{\beta}_k$ are

$$\tilde{\beta}_1 = \frac{a(\bar{\rho} \bar{V} - \bar{\rho} v)}{2\sqrt{\frac{C}{\rho}}} \quad \text{and} \quad \tilde{\beta}_2 = \frac{a(\bar{\rho} v - \bar{\rho} \bar{V})}{2\sqrt{\frac{C}{\rho}}} \quad (5.6)$$

We are now in a position to use the Roe Scheme to calculate the component by component discrete problem in each cell. Then the results are recombined to give the full solution to the non-linear system.

5.2 The Roe Scheme

The first order upwind scheme with Roe decomposition is known as the Roe scheme. A numerical scheme approximates the solution to a problem in (x, t) space. We decompose the data over discrete, uniform cells of dimensions Δx in space and Δt in time. The information is given at the end points of each cell such that the approximation $\mathbf{u}_j^{n+1} \approx \mathbf{u}(j\Delta x, n\Delta t)$ the exact solution. Here j denotes the point in x -space and n in t -space, where $j = 0, \dots, J$ and $n = 0, \dots, N$.

The first order upwind scheme approximates the time derivative by the one-sided difference

$$\mathbf{u}_t \approx \frac{\mathbf{u}_j^{n+1} - \mathbf{u}_j^n}{\Delta t}.$$

Coupled with the Roe averages the conservation form can be written

$$\mathbf{u}_j^{n+1} = \mathbf{u}_j^n - \frac{\Delta t}{\Delta x} \Delta \mathbf{f} + \Delta t \mathbf{R}$$

which is

$$\mathbf{u}_j^{n+1} = \mathbf{u}_j^n - \frac{\Delta t}{\Delta x} \sum_{k=1}^2 \tilde{\alpha}_k \tilde{\lambda}_k \tilde{\mathbf{r}}_k + \Delta t \sum_{k=1}^2 \tilde{\beta}_k \tilde{\mathbf{r}}_k.$$

The update over the j^{th} cell depends on the wave speeds λ_k such that

$$\mathbf{u}_j^{n+1} = \mathbf{u}_{j+1}^n - \frac{\Delta t}{\Delta x} \tilde{\alpha}_k \tilde{\lambda}_k \tilde{\mathbf{r}}_k + \Delta t \tilde{\beta}_k \tilde{\mathbf{r}}_k.$$

if $\tilde{\lambda}_k < 0$, and

$$\mathbf{u}_j^{n+1} = \mathbf{u}_j^n - \frac{\Delta t}{\Delta x} \tilde{\alpha}_k \tilde{\lambda}_k \tilde{\mathbf{r}}_k + \Delta t \tilde{\beta}_k \tilde{\mathbf{r}}_k.$$

if $\tilde{\lambda}_k > 0$.

5.2.1 Accuracy and Stability

Roe uses the first order upwind scheme to approximate the data, and so is first order accurate in both time and space. A solution will have an error of order Δt in time and order Δx in space. The accuracy is found by expanding the one sided approximations to the derivatives using Taylor series about the point (x_j, t_n) .

In order for the numerical method to be stable we require

$$\frac{\Delta t}{\Delta x} |\max_{k=1,2} \lambda_k| < 1$$

over all j . This ensures that any wave will only travel through a single cell at each time step.

5.2.2 Boundary Conditions

We need to impose boundary conditions at the left and right ends where the waves travel out of the domain. At the left hand end $j = 0$ and \mathbf{u}_0^{n+1} will not be updated by a downwind wave from the previous cell as this cell does not exist. Since the data is constant here we can update \mathbf{u}_0^{n+1} by overwriting it with \mathbf{u}_1^{n+1} . Similarly we set the boundary condition at $j = J$ by overwriting \mathbf{u}_J^{n+1} with \mathbf{u}_{J-1}^{n+1} .

5.3 The Data

In Section 4.1 we used initial data given in [8]. We again use these step functions for initial ρ and v , but now we must find suitable values for a, C, \bar{V} and Δx and Δt .

We take the relaxation term a to be small, about 0.1 as this governs how much effect the large optimal velocity $\bar{V} \approx 1$ (in the case where \bar{V} is constant) has on the system. The values of C was chosen by running the homogeneous program and comparing the results with the Riemann solution. After some trial and error $C = 0.05$, since this generated results closest to what was expected.

The following chapter discusses the numerical results of the homogeneous program and the inhomogeneous programs with \bar{V} constant, $V(\rho) = \tanh(\rho - 2) - \tanh(-2)$, as in Bando [1], and the similarity solution.

Chapter 6

Numerical Results

6.1 The Homogeneous System

Firstly we consider the numerical results of the homogeneous system

$$\begin{aligned}\rho_t(\rho v)_x &= 0 \\ v_t + vv_x - Cb_x &= 0.\end{aligned}$$

The program was run with $a = 0$ for varying values of Δx and Δt . As in the Riemann solution we expect to see two shocks travelling with different speed and direction. Figure 6.1 shows the 2-shock in front of the discontinuity moving to the right with a greater speed than the 1-shock (only just visible) moves to the left. The over-shoot in initial ρ represents the point ρ_M , as in \mathbf{u}_M . We see that the 2-shock is slightly diffused, probably due to the low accuracy of the first order scheme. We re-run the program with the larger space step $\Delta x = 0.5$. This gives a better indication of the 1-shock moving quickly, backwards to the left and the other shock, in front of the discontinuity. This is shown in Figure 6.2 and Figure 6.3 where $\Delta t = 0.01$.

What does this tell us in terms of the vehicles on the road? To the left of the discontinuity the headway is large and so all the cars are able to travel with a high constant velocity. As these cars approach the congestion (represented by the discontinuity) they are forced to slow down rapidly. More

cars approach from behind and must slow down sooner, thus we see the congestion (high density) propagates backwards along the road. As the cars enter the congested region the density increases slightly, where drivers ‘ease off’ on the brakes, so deceleration is slower, and thus the headway of the cars approaching from behind decreases. The cars then slow down to the lower constant velocity. At the right hand end all the cars are travelling at a low speed because the headway is small.

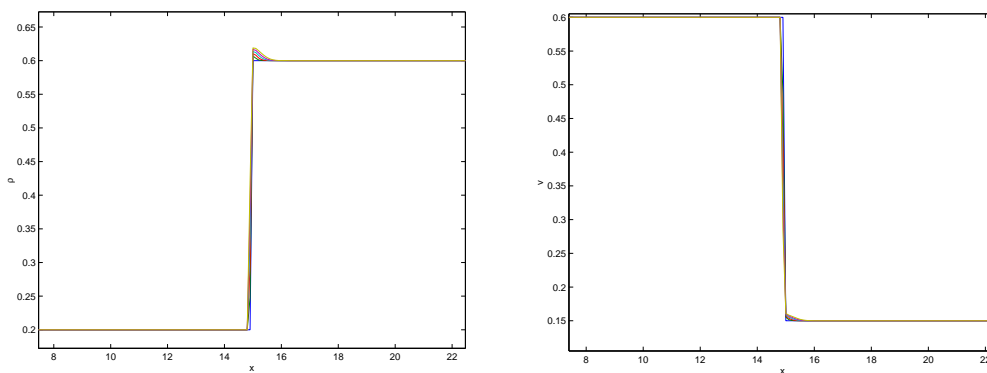


Figure 6.1: $a = 0$, $\Delta x = 0.1$, $\Delta t = 0.001$. Every 200th time step to $t = 1$.

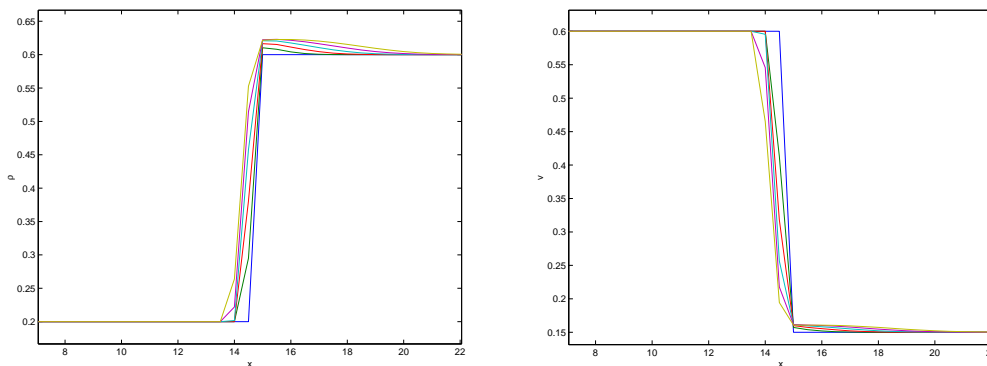


Figure 6.2: $a = 0$, $\Delta x = 0.5$, $\Delta t = 0.01$. Every 200th time step to $t = 10$.

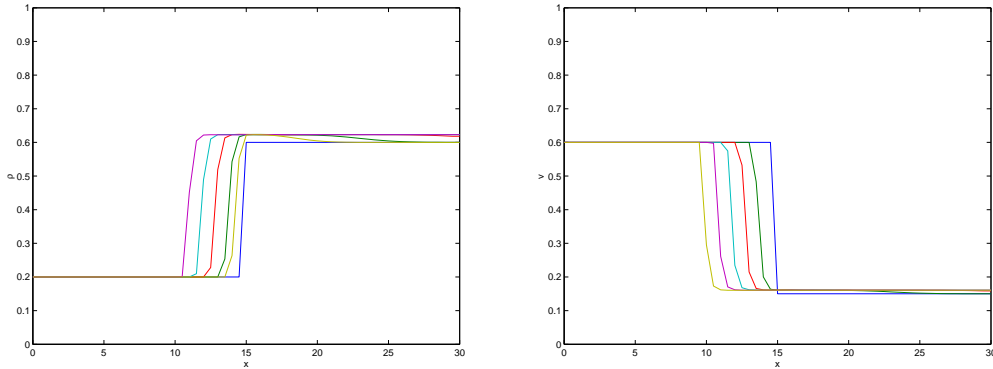


Figure 6.3: $a = 0$, $\Delta x = 0.5$, $\Delta t = 0.01$. Every 2000th time step to $t = 100$.

6.2 The Inhomogeneous System

Now we consider the inhomogeneous system

$$\begin{aligned}\rho_t(\rho v)_x &= 0 \\ v_t + vv_x - Cb_x &= a(\bar{V}(\rho) - v).\end{aligned}$$

We run two programs, one where \bar{V} is constant and the second where it is a function of ρ .

6.2.1 Constant \bar{V}

The program was run with $\Delta t = 0.01$ for 1000 time steps and various values of \bar{V} and a . Figure 6.4, where $a = 0.1$, $\bar{V} = 0.9$ and $\Delta x = 0.3$ (therefore, only 60 space steps), shows the constant velocity to the left of the discontinuity increasing with time as cars here can accelerate, uniformly in space, with each time step to the optimal velocity, \bar{V} , since there is no change in the headway. Here the density is low and so the headway is large. When the vehicles reach the congestion they decelerate rapidly as before. Now, however, the density does not propagate backwards. The cars at the right hand state increase their constant velocity, with each time step, towards \bar{V} . The cars behind these adjust their speed and start to accelerate to reach the

same velocity. This causes the region of high density to move forward with each time step.

Figure 6.5 refines the space step size of the previous figures and gives a smoother representation. Figure 6.6 is the case when $a = 0.5$ and so the source term has a larger effect on the solution. The density behaves like the previous situation after a large time, as we would expect. The smooth curve represents a uniform change in the headway as cars in low density meet those in high density. The velocity plot shows the cars are indeed reaching the optimal velocity. Figure 6.7 is the case where $a = 0.1$ and $\bar{V} = 0.5$. If the optimal velocity is small compared to the initial velocity the cars in constant density decelerate with each time step. The cars with smaller initial velocity will accelerate to reach \bar{V} at a faster rate.

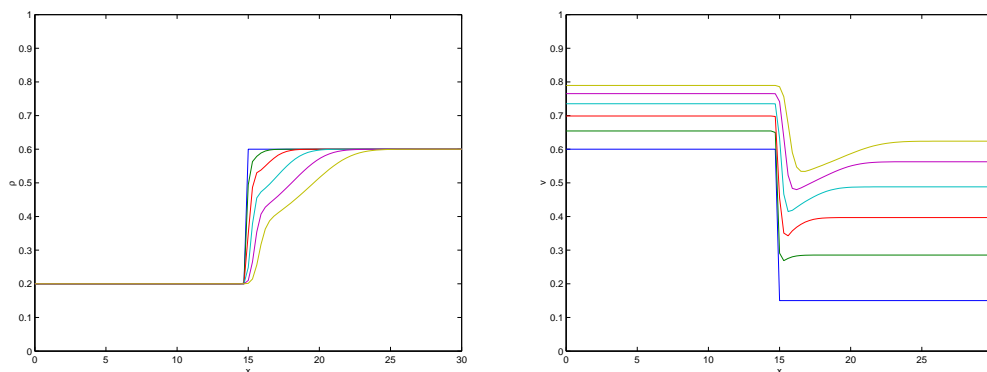


Figure 6.4: $a = 0.1$, $\bar{V} = 0.9$, $\Delta x = 0.3$, $\Delta t = 0.01$. Every 200th time step to $t = 10$.

6.2.2 Function $\bar{V}(\rho)$

The program was also run with the dynamic equation

$$\bar{V}(\rho) = \tanh(\rho - 2) - \tanh(-2).$$

However, the numerical scheme fails here giving increasing values of v and ρ . Figure 6.8 shows the solution when $\Delta x = 0.3$, $\Delta t = 0.02$ and $a = 0.1$ so the contribution from the source term is small. Recall that the initial data

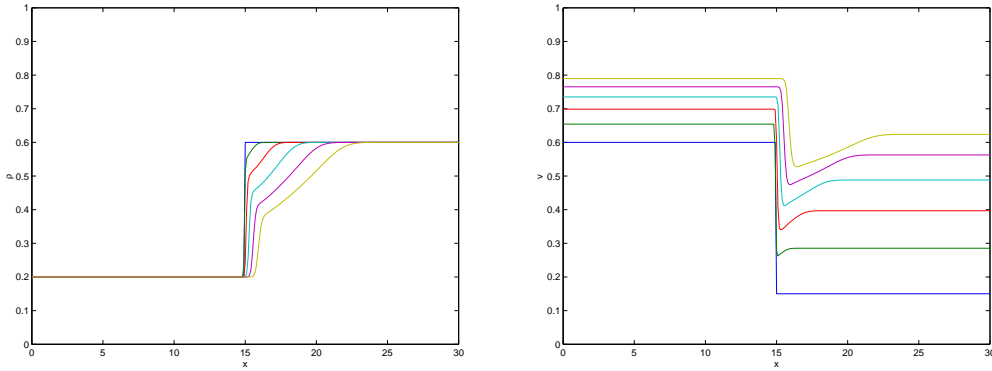


Figure 6.5: $a = 0.1$, $\bar{V} = 0.9$, $\Delta x = 0.1$, $\Delta t = 0.01$. Every 200th time step to $t = 10$.

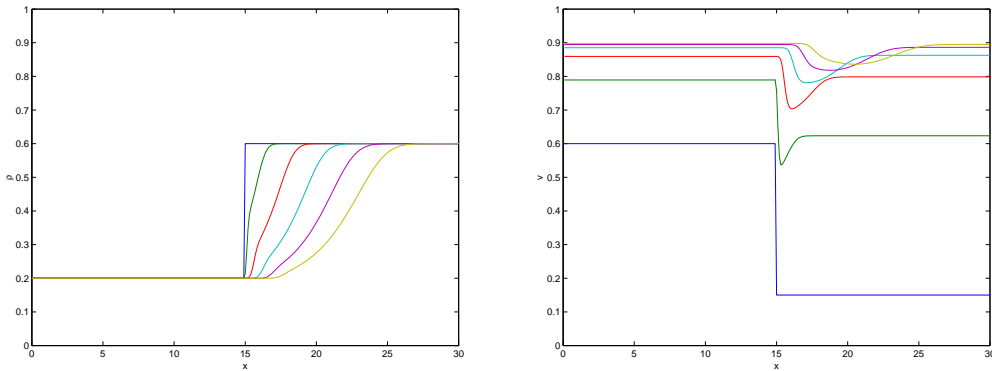


Figure 6.6: $a = 0.5$, $\bar{V} = 0.9$, $\Delta x = 0.3$, $\Delta t = 0.01$. Every 200th time step to $t = 10$.

has been normalised and so $\rho < 1$ is not a physically possible solution. As a increase the maximum values of v and ρ do also.

6.3 The Similarity Solution

We run the inhomogeneous program with $x = \xi$ and $v = \check{v}$. This gives the system

$$\begin{aligned} \rho_t + (\rho v)_\xi &= 0 \\ v_t + v\check{v}_\xi - Cb_\xi &= a(\bar{V} - \check{v}) \end{aligned}$$

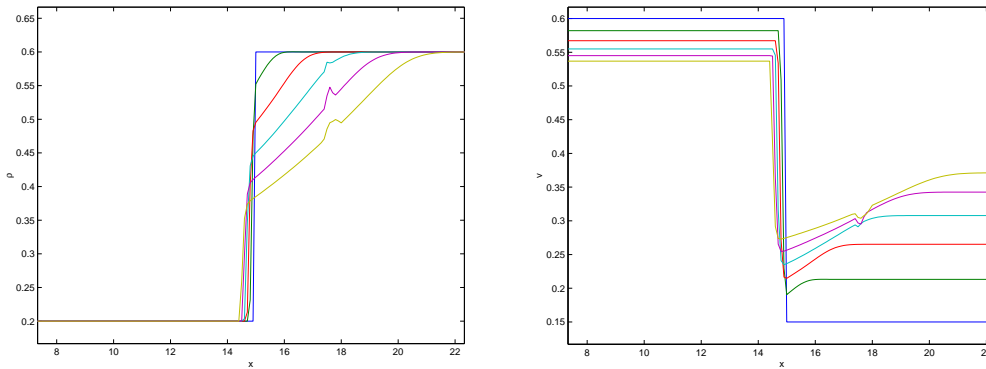


Figure 6.7: $a = 0.1$, $\bar{V} = 0.5$, $\Delta x = 0.3$, $\Delta t = 0.01$. Every 200th time step to $t = 10$.

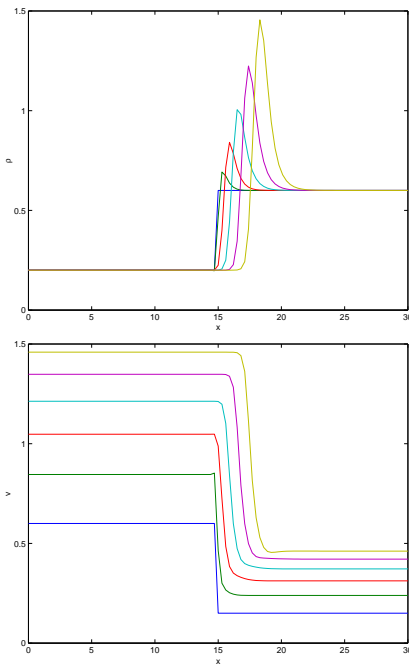


Figure 6.8: $a = 0.1$, $\bar{V} = 0.9$, $\Delta x = 0.3$, $\Delta t = 0.01$. Every 200th time step to $t = 10$.

and setting $\bar{V} = 0$ we can compare the results with the similarity solution.

In Figure 6.9 we see that given any initial data the solution of $\check{v} \rightarrow 0$. This confirms our previous solution that the system tends towards the optimal velocity as $t \rightarrow 0$.

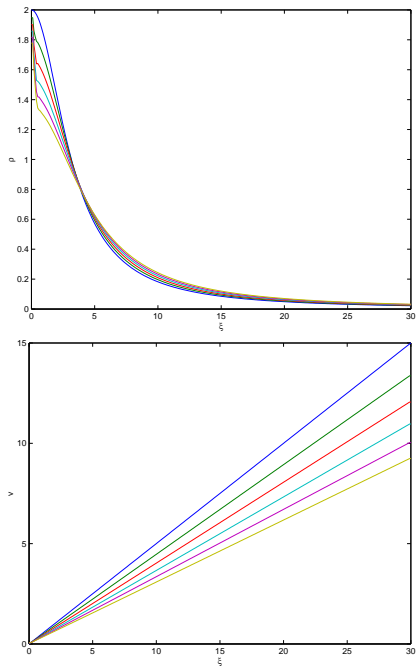


Figure 6.9: $a = A = 1$, $\bar{V} = 0$, $\Delta\xi = 0.1$, $\Delta t = 0.01$. Every 200th time step to $t = 10$.

Chapter 7

Conclusions and Further Work

The aim of this dissertation has been to develop a macroscopic traffic flow model from a microscopic model and to solve it numerically. We based our dynamic equation on Bando [1] and introduced an extra term governing change in the headway.

A moving coordinate system is used to find a similarity solution to the inhomogeneous model. The behaviour of the solutions approach the fixed point $(\rho_0, f) = (0, 0)$ as $t \rightarrow 0$. Thus the source term has a large effect on the model causing the speed of the cars to approach the optimal velocity \bar{V} . These results are also given by the numerical method.

The homogeneous system is considered with initial data giving a single discontinuity. This Riemann problem gives two shock waves. The Roe decomposition coupled with the first order upwind scheme allows us to write a program to numerically model the homogeneous system accurately. The inhomogeneous system contains some instability probably due to the first order accuracy yet still shows the cars reaching the optimal velocity when the density is constant.

The Roe scheme was not able to cope with the situation where the optimal velocity is dependent on the density as in Bando. It would be of interest to use higher order numerical schemes to model the system more accurately.

Overall, the model works well if there is no source term. However, real-

istically the optimal velocity *is* dependent on the density. Since, in constant density, it would be foolhardy to drive at the same optimal velocity for congested traffic as one would in light traffic flow.

Another refinement is to assume that C is also a function of the density ρ and to develop a system that switches between two sub-problems at a defined value of the headway. By these means we would hope to model the way the traffic accelerates in low density and maintains a lower steady speed in high density.

Bibliography

- [1] M.Bando *et al.*, *Dynamical model of traffic congestion and numerical simulation*, *Phy Rev E*, 51, pp 1035 – 1042 (1995).
- [2] M.J.Lighthill & G.B. Whitam *On kinematic waves. II. A theory of traffic flow on long crowded roads* *Proc. Royal Soc.*, A229, pp 281 – 345 (1955)
- [3] G.B. Whitam *Linear and Nonlinear Waves* John Wiley, New York, (1974)
- [4] B.S. Kerner & P. Konhäuser *Structure and parameters of clusters in traffic flow* *Phys Rev E*, 50, pp 54 – 83 (1994)
- [5] P. Berg, A. Mason & A. Woods *Continuum approach to car-following models* *Phys Rev. E*, 61, pp1056 – 1066 (2000)
- [6] H.M. Zhang *A non-equilibrium traffic model devoid of gas-like behaviour* *Transpn Res. B* 36, pp 275 – 290 (2002)
- [7] A. Aw & M. Rascle *Ressurrection of ‘second order’ models of traffic flow?* *SIAM J. Appl. Math.*, 60, pp 916 – 938 (2000)
- [8] J.V. Morgan *Numerical Methods for Macroscopic Traffic Models* PhD Thesis, University of Reading (2002)
- [9] J.V. Morgan, M.J. Baines & P.K. Sweby *Roe Decomposition and a Test Problem for Macroscopic Motorway Traffic Models* unpublished report, (2003)

- [10] Y.C. Tai, S. Noelle, J.M.N.T. Gray & K. Hunter *Shock-Capturing and Front-Tracking Methods for Granular Avalanches* Journal of Computational Physics 175, pp269 – 301 (2001)
- [11] R.J. Leveque *Finite Volume Methods for Hyperbolic Problems* Cambridge University Press (2002)
- [12] P.K.Sweby *Numerical Techniques for Conservation Laws* course notes for M.Sc. module, (2003)